https://doi.org/10.1016/j.scriptamat.2016.09.016

Sintering temperature dependence of thermoelectric performance in $CuCrSe_2$ prepared via mechanical alloying

Yanci Yan[a], Lijie Guo[a], Zhi Zhang[c], Xu Lu[a], Kunling Peng[a,b], Wei Yao[a], Jiyan Dai[c], Guoyu Wang[b], Xiaoyuan Zhou[a]*

[a]College of Physics, Chongqing University, Chongqing 401331, People's Republic of China.

[b]Chongqing Institute of Green and Intelligent Technology, Chinese Academy of Sciences, Chongqing 400714, People's Republic of China.

[c]Department of Applied Physics, The Hong Kong Polytechnic University, Kowloon, Hong Kong, China

Abstract:

$CuCrSe_2$ compounds were synthesized by mechanical alloying followed by annealing and spark plasma sintering at temperatures of 873*K*, 923*K*, 973*K* and 1023*K*. Our investigation revealed that high spark plasma sintering temperature (above 973*K*) is the key to obtaining $CuCrSe_2$ single phase completely free of a metallic secondary phase $CuCr_2Se_4$. The ultralow thermal conductivity caused by the Cu ions disorder, complex layered structure and dislocation leads to the favorable thermoelectric performance in $CuCrSe_2$ compound. A maximum dimensionless figure of merit *ZT* value over 0.75@873 *K* is achieved in the absolutely pure sample sintered at 1023*K*.

Keywords: $CuCrSe_2$, single phase, layered structure, PLEC

With the rapid development of society, growing energy consumption has led to the emission of more greenhouse gas and pollutants [1-2]. To resolve the environmental issues, the Chinese government has issued new green energy policies to encourage more efficient utilization of energy. Thermoelectricity, which can directly covert heat into electricity, opens a promising path for recovering the lost energy in industrial and automobile waste heat [3-5]. The efficiency of thermoelectric conversion is defined by a dimensionless figure of merit, $ZT=S^2\sigma T/\kappa$, where S is the Seebeck coefficient, σ is the electrical conductivity, T is the absolute temperature, and κ is the total thermal conductivity. The total thermal conductivity can be further decomposed to contributions from the lattice part (κ_L) and the electronic part (κ_e), where for metals and degenerate semiconductors $\kappa_e=L\sigma T$ (L is Lorenz number). A good thermoelectric material should have both a high power factor (PF) σS^2 and low thermal conductivity.

Although the expression of ZT is simple, S, σ and κ_e are all functions of the carrier concentration, and hence are strongly coupled with each other [6-7]. Virtually none of these properties can be independently tuned for achieving a high ZT, but the lattice thermal conductivity κ_L is the only term that is governed by a material's structural features. It has been reported that many state-of-the-art thermoelectric materials feature complex structures, such as Cu-based compounds [8-9] , SnSe [10-12], In_4Se_3 [13], where strong intrinsic phonon scattering gives rise to ultralow thermal conductivity and hence high ZT values.

These materials inspired a novel concept in the thermoelectric known as phonon glass and electron crystal (PGEC), which means good thermoelectric materials should

possess low κ like glassy materials but high σ (low ρ) like crystalline semiconductors [14]. Since then, many PGEC have been extensively studied by researchers such as: CoSbS [15], Cu_2Se [16], $AgCrSe_2$ [17], and $CuCrSe_2$ [18-19] etc. Recently, $CuCrSe_2$, an ionic-electronic conductor, has regained popularity for its phonon-liquid electron-crystal (PLEC) transport behaviors. $CuCrSe_2$ features a layered structure composed by CdI_2 type $CrSe_2^-$, in which the Cr^{3+} cations are surrounded by the Se^{2-} anions that form a distorted octahedral coordination sphere. Between the $CrSe_2^-$ layers, the interlayer space is occupied by Cu ions. The Cu ions are disordered in this structure, occupying two different tetrahedral sites. At low temperatures Cu ions only occupy one of the tetrahedral sites while Cu ions begin to migrate to other tetrahedral site at a transition temperature round 365 *K* [18-19]. The strong disorder of Cu ions in the $CuCrSe_2$ is expected to result in low thermal conductivity like that of glassy materials. At room temperature, $CuCrSe_2$ has a band gap E_g = 0.157eV [19], which conforms to the selection rule of having a narrow band gap for good thermoelectric materials. Recently, S. Bhattacharya *et al* synthesized $CuCrSe_2$ via solid state reaction and reported a peak *ZT* of 0.25 at 773*K* [18]; Meanwhile, it is worth to mention that there is no sign of anisotropy in $CuCrSe_2$ compound with layered structure [19].

In spite of its promising attributes for TE applications, it is extremely difficult to obtain a pure phase of $CuCrSe_2$ due to its complex phase transitions during solidification. As shown in the phase diagram of Fig.S1, the $CuCrSe_2$ prepared by conventional vacuum melting and solidification contains the second phase of $CuCr_2Se_4$. To overcome the synthesis challenge, we resorted to mechanical alloying (MA) [20-22] followed by

vacuum annealing. After that, $CuCrSe_2$ ingot was pulverized and sintered into bulk samples by SPS. By properly controlling the SPS sintering temperature, we have successfully obtained totally single phase $CuCrSe_2$ that possesses thermal conductivity lower than that reported in previous works [18-19]. We believe the ultralow thermal conductivity of these SPS samples originates from the intrinsic layered structure combined with Cu ions disorder and dislocations within a crystalline solid.

High-purity elemental powders of Cu(99.99%), Cr(99.9%) and Se(99.99%) were weighed according to the stoichiometric ratio. All constituents were loaded into a planetary ball mill (*Pulverisette 7*) placed in the glove box. Tungsten carbide vessel and corresponding balls were used, and the weight ratio of ball to powder was kept at 10:1. The powders were mechanically alloyed for 8h at 500 rpm, which was found to be the optimum MA condition for the synthesis and thermoelectric performance of $CuCrSe_2$. The as-milled powders were sealed in quartz ampoules under vacuum of ~7.8×10^{-4}mbar, slowly heated to 1173 *K* in 20 h and kept at such temperature for 72h before cooling down to room temperature. The ingots obtained were re-grounded into fine powder and then sintered into dense pellets by SPS (*SPS-625*) under 50 MPa at varying temperatures (873–1023 *K*) for 5 min in a graphite die. The densities of final products are greater than 95% of the theoretical density.

The obtained pellets were cut into about 9 mm×3 mm ×3 mm rectangular parallelepipeds for electrical property measurements and round disks of 10 mm in diameter and about 1 mm in thickness for thermal conductivity measurement. Seebeck coefficient and electrical conductivity were measured using LSR-3 (*Linseis, Germany*)

instrument measuring system under a static helium atmosphere. The thermal conductivity is determined by $\kappa=\rho DC_p$, where ρ is the density measured using the mass and geometric volume of the pellet, the thermal diffusivity(D) measured by a Netzsch 457 (*Netzsch, Germany*) microflash LFA system, and specific heat C_p measured using a *Netzsch, 404 F3*. As mentioned in the introduction, the lattice thermal conductivity was obtained by $\kappa_L=\kappa-\kappa_e$. where κ_e is estimated by Wiedemann-Franz law $\kappa_e=\sigma LT$. The errors in the measurements of electrical conductivity, Seebeck coefficient, thermal diffusivity, and C_p are about 5%, 5%, 3%, and 3%, respectively. All thermoelectric properties were measured from 300*K* to 873*K*. Powder x-ray diffraction (XRD) patterns were collected from powders using a PANalytical X'Pert apparatus with Cu Kα radiation. A scanning electron microscope (*JSM-7800F, JEOL*) was used to image the morphology. The verification of the crystal structure was carried out by transmission electron microscopy (*TEM, JEOL 2100F*).

Fig .1 shows the XRD patterns of all bulk $CuCrSe_2$ samples after SPS at different temperatures. All major reflections of the polycrystalline samples are indexed to the $CuCrSe_2$ phase. A small amount of secondary phase $CuCr_2Se_4$ was found in samples sintered at 873*K* and 923*K*. When the sintering temperature reached 973*K* and above, the secondary phase disappeared and single phase of $CuCrSe_2$ was successfully obtained.

Figs. 2a-b display the scanning electron microscope (SEM) images of the cross section of samples sintered at 873*K* and 1023*K*. It is the evident that all samples are of intrinsic layered structures, but the bulk polycrystalline samples show no sign of anisotropy [19].

As shown in Figs. 2a-b, it is apparent that the grains are closely packed, which is in agreement with the measured high density of our bulk samples. Figs. 2c-d are transmission electron microscope (TEM) images of $CuCrSe_2$ compound sintered at 1023*K* and Figs. 2e-f are for the sample sintered at 873*K*. In Fig. 2c, one can see that there are many dislocations present in the grains. To illustrate their crystal structures, high-resolution TEM images and selected area electron diffraction (SAED) patterns were taken. Fig. 2d is a typical high-resolution TEM image, indicating the hexagonal crystal structure and lattice spacing of $CuCrSe_2$, which is further confirmed by the SAED pattern in the inset. Similar TEM investigations were performed on the sample sintered at 873K, and Fig. 2e shows the bright-field TEM image with clear grain boundaries. Our detailed high-resolution TEM images prove the hexagonal crystal structure and lattice spacing of $CuCrSe_2$ as well. In addition, a secondary phase of $CuCrSe_4$ with cubic structure was also founded in this sample, as demonstrated in the Fig. 2f and its inset. This is in excellent consistence with the XRD results.

The electrical conductivity, Seebeck coefficient and the calculated power factors are shown in Figs. 3a-c. Abnormalities around 365 *K* in the electrical and thermal transport data indicate the onset of the disorder of Cu ions. Below 365*K*, the sharp decrease of electrical conductivity with increasing temperature is indicative of a typical degenerate semiconductor. As temperature rises above 365*K*, the electrical conductivity shows a very weak temperature dependence, which resembles the high temperature behavior of an ionic semiconductor such as $AgCrSe_2$ [17]. The electrical conductivity of samples sintered at 873*K* and 923*K* are in agreement with the previously reported values [18-

19] and much higher than those sintered at 973*K* and 1023*K* due to the presence of the metallic secondary phase $CuCr_2Se_4$. The reason why samples sintered at 873*K* and 923*K* has higher electrical conductivity is attributed to the carrier concentration enhancement. As shown in Table I, the carrier concentration for samples sintered at 873*K* and 923*K* are much higher than samples sintered at 973*K* and 1023*K*. Although the presence of second phase $CuCr_2Se_4$ in $CuCrSe_2$ samples sintered at 873*K* and 923*K* may result in the reduction of carrier mobility, the increase of carrier concentration far exceeds the reduction of carrier mobility, yielding the improvement of electrical conductivity in samples sintered at 873*K* and 923*K*.

Fig. 3b shows the temperature dependence of Seebeck coefficient. The positive sign of S implies all samples are intrinsic p-type semiconductors. For samples sintered at 873*K* and 923*K*, the Seebeck coefficient decreases from room temperature to about 365*K* and then steadily increases from 80$\mu V/K$ at 365*K* to 140$\mu V/K$ at 873*K*. The Seebeck coefficients of samples sintered at 973*K* and 1023*K* exhibit a similar trend: decreasing from room temperature and then becoming almost temperature independent. In addition, the value of Seebeck coefficient increases with the decrease of carrier concentration, however, it decreases with the decreases of effective mass for similar carrier concentration as shown in Table I. It is noted that the band gap of $CuCrSe_2$ is 0.157eV [19], the activation of minority carriers play negative effects on Seebeck coefficient above 600*K*. This behavior and values of Seebeck coefficient have not been observed in previously published work on $CuCrSe_2$ [18-19]. Fig. 3c displays the calculated power factors. Because of the reduced electrical conductivity, the peak power factors of pure

single phase $CuCrSe_2$ samples are lower than those of samples containing the metallic secondary phase.

Fig. 4a displays the temperature dependence of total thermal conductivity κ of bulk $CuCrSe_2$ samples. From 300 K to 365 K, the reduction of κ is attributed to the disorder of Cu ions. Above 365 K, thermal conductivity becomes nearly temperature independent as amorphous materials. The total thermal conductivity, especially that of samples sintered at 973K and 1023K, is extremely low even compared with other well-known thermoelectric materials with intrinsically low thermal conductivity [8-13]. This could be contributed to the following synergistic phonon scattering mechanisms: (a) dislocations proved by TEM attribute to the extremely low total thermal conductivity; (b) the phonons with a larger mean free path of several mms are scattered by micron-size layered grain structure; (c) the property of a superionic conductor with liquid like substructures (i.e. diffusion of ions within the crystalline sublattice) also attributes to ultralow thermal conductivity by reducing the phonon mean free path and eliminating some of the phonon vibration modes [23]. Besides, the lower values of total thermal conductivity of samples sintered at 973K and 1023K is caused by reduced electrical thermal conductivity (inset). It should be noted that the total thermal conductivity for samples sintered at 873K and 923K shows good consistency with other independently reported values [18-19]. The temperature dependence of lattice thermal conductivity are shown in Fig. 4b which is calculated by subtracting the electronic thermal conductivity from the total thermal conductivity. The Lorenz number L, which depends on the degree of elasticity in carrier scattering, can be calculated by Equation (1):

$$L = \left(\frac{k_B}{e}\right)^2 \left[\frac{\left(r+\frac{7}{2}\right)F_{r+\frac{5}{2}}(\xi)}{\left(r+\frac{3}{2}\right)F_{r+\frac{1}{2}}(\xi)} - \left(\frac{\left(r+\frac{5}{2}\right)F_{r+\frac{3}{2}}(\xi)}{\left(r+\frac{3}{2}\right)F_{r+\frac{1}{2}}(\xi)}\right)^2\right] \quad (1)$$

where the scattering factor r is the exponent of the energy dependence on the charge carrier mean free path. For acoustic phonon scattering in the $CuCrSe_2$ system, r takes a value of −1/2. Fn(ξ) is the Fermi integral defined as:

$$F_n(\xi) = \int_0^\infty \frac{x^n}{1 + e^{x-\xi}} dx \quad (2)$$

where ξ is the reduced Fermi energy that can be deduced from the Seebeck coefficient and the scattering factor based on the following formula assuming a single parabolic band:

$$s = \pm \frac{k_B}{e}\left(\frac{\left(r+\frac{5}{2}\right)F_{r+\frac{3}{2}}(\xi)}{\left(r+\frac{3}{2}\right)F_{r+\frac{1}{2}}(\xi)} - \xi\right) \quad (3)$$

The lattice component κ_L as a function of temperature is plotted in Fig. 4b and the inset in Fig. 4b shows κ_e of all samples. Overall, the lattice component κ_L for all samples are extremely low due to the complex layered structure combined with PLEC mechanism. In the end, it is worth mentioning that the observed high temperature κ of $CuCrSe_2$ is comparable to various recently reported ionic semiconductors such as $AgCrSe_2$ [17], Zn_4Sb_3 [24-26] and Cu_2Se [16], showing advantages of layered structure combined with PLEC mechanism.

Fig. 4d shows the temperature dependence of *ZT* values of SPS samples. Although the maximum *ZT* values of sample sintered at 873*K* and 1023*K* show little difference, the average *ZT* value of sample sintered at 1023*K* is higher. Since the efficiency of thermoelectric device is determined by the average *ZT* of constituent materials, the SPS

sample prepared at 1023*K* has an advantage over the one prepared at lower temperatures for waste heat recovery applications. In addition, compared with other ionic semiconductors possessing intrinsic low thermal conductivity [17], $CuCrSe_2$ shows excellent thermoelectric performance regardless of SPS temperature.

In this study, via mechanical alloying followed by annealing and spark plasma sintering, we have successfully synthesized pure single phase $CuCrSe_2$ polycrystalline compounds. Our investigation focused on the temperatures dependence of SPS on the thermoelectric performance in $CuCrSe_2$ based compounds. It is found that high SPS temperature (above 973*K*) plays a vital role for obtaining pure single phase $CuCrSe_2$. In addition, disorder of Cu ions and complex layered structure combined with dislocations contribute to the ultralow thermal conductivity while maintaining a reasonable power factor. A peak *ZT* up to 0.75 @873*K* was obtained in the completely pure sample sintered at 1023*K*.

Acknowledgements

This work was financially supported in part by the National Natural Science Foundation of China (Grant Nos. 11404044, 51472036). The work conducted at the Chongqing Institute of Green and Intelligent Technology, Chinese Academy of Sciences is supported by the 100 Talent Program of the Chinese Academy of Sciences (Grant No. 2013-46) and the National Natural Science Foundation of China (Grant No. 11344010).

[1] M. Wise, K. Calvin, A. Thomson, L. Clarke, B. Bond-Lamberty, R. Sands, S. J. Smith, A. Janetos and J. Edmonds, Science. 324 (2009) 1183-1186.

[2] T. Wheeler and J. von Braun, Science. 341 (2013) 508-513.

[3] X. Y. Zhou, G. W. Wang, L. J. Guo, H. Chi, G. Y. Wang, Q. F. Zhang, C. Q. Chen, T. Thompson, J. Sakamoto,V. P. Dravid, G. Z. Cao and C. Uher, J Mater Chem A. 2 (2014) 20629-20635.

[4] X. Lu, D. T. Morelli, Y. Xia, F. Zhou, V. Ozolins, H. Chi, X. Y. Zhou and C. Uher, Adv Energy Mater. 3 (2013) 342-348.

[5] Q. F. Chen, G. W. Wang, A. J. Zhang, D. F. Yang, W. Yao, K. L. Peng, Y. C. Yan, X. N. Sun, A. P. Liu,G.Y. Wang and X. Y. Zhou, J Mater Chem C. 3 (2015) 12273-12280.

[6] A. F. Ioffe, Semiconductor thermoelements, and Thermoelectric cooling, Infosearch, London, 1957

[7] G. J. Snyder and E. S. Toberer, Nat Mater. 7 (2008) 105-114.

[8] P. F. Qiu, T. S. Zhang, Y. T. Qiu, X. Shi and L. D. Chen, Energ Environ Sci. 7 (2014) 4000-4006.

[9] X. Lu and D. T. Morelli, Phys Chem Chem Phys. 15 (2013) 5762-5766.

[10] L. D. Zhao, S. H. Lo, Y. S. Zhang, H. Sun, G. J. Tan, C. Uher, C. Wolverton, V. P. Dravid and M. G. Kanatzidis, Nature. 508 (2014) 373-+.

[11] J. D. Wasscher, W. Albers and C. Haas, Solid State Electron. 6 (1963) 261-264.

[12] K. L. Peng, X. Lu, H. Zhan, S. Hui, X. D. Tang, G. W. Wang, J. Y. Dai, C. Uher, G. Y. Wang and X. Y. Zhou, Energ Environ Sci. 9 (2016) 454-460.

[13] J. S. Rhyee, K. H. Lee, S. M. Lee, E. Cho, S. Il Kim, E. Lee, Y. S. Kwon, J. H. Shim and G. Kotliar, Nature. 459 (2009) 965-968.

[14] D. M. Rowe and G. Min, Iee P-Sci Meas Tech. 143 (1996) 351-356.

[15] D. Parker, A. F. May, H. Wang, M. A. McGuire, B. C. Sales and D. J. Singh, Phys Rev B 87(2013).

[16] S. Ballikaya, H. Chi, J. R. Salvador and C. Uher, J Mater Chem A. 1 (2013) 12478-12484.

[17] F. Gascoin and A. Maignan, Chem Mater. 23 (2011) 2510-2513.

[18] S. Bhattacharya, R. Basu, R. Bhatt, A. Singh, D. K. Asw and S. K. Gupta, Proceeding of International Conference on Recent Trends in Applied Physics & Material Science. (Ram 2013) 1536 (2013) 1233-1234.

[19] S. Bhattacharya, R. Basu, R. Bhatt, S. Pitale, A. Singh, D. K. Aswal, S. K. Gupta, M. Navaneethan and Y. Hayakawa, J Mater Chem A. 1 (2013) 11289-11294.

[20] W. S. Liu, B. P. Zhang, J. F. Li and L. D. Zhao, J Phys D Appl Phys. 40 (2007) 566-572.

[21] A. Zevalkink, W. G. Zeier, E. Cheng, J. Snyder, J. P. Fleurial and S. Bux, Chem Mater. 26 (2014) 5710-5717.

[22] A. Zevalkink, E. S. Toberer, W. G. Zeier, E. Flage-Larsen and G. J. Snyder, Energ Environ Sci. 4 (2011) 510-518.

[23] H. L. Liu, X. Shi, F. F. Xu, L. L. Zhang, W. Q. Zhang, L. D. Chen, Q. Li, C. Uher, T. Day and G. J. Snyder, Nat. Mater. 11 (2012), 422.

[24] F. Cargnoni, E. Nishibori, P. Rabiller, L. Bertini, G. J. Snyder, M. Christensen, C. Gatti and B. B. Iversen,Chem-Eur J. 10 (2004) 3861-3870.

[25] G. J. Snyder, Appl Phys Lett. 84 (2004) 2436-2438.

[26] E. S. Toberer, P. Rauwel, S. Gariel, J. Tafto and G. J. Snyder, J Mater Chem. 20 (2010) 9877-9885.

Captions for Figures

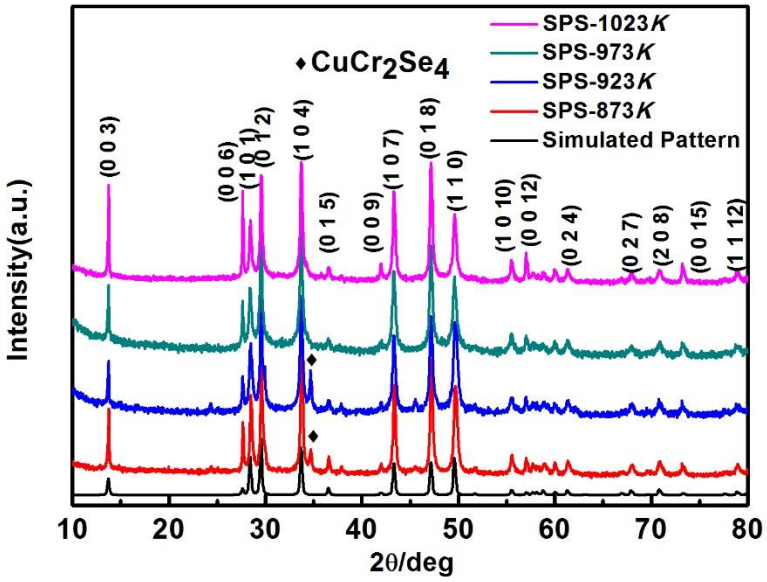

Fig. 1 XRD patterns of $CuCrSe_2$ after SPS at different temperatures.

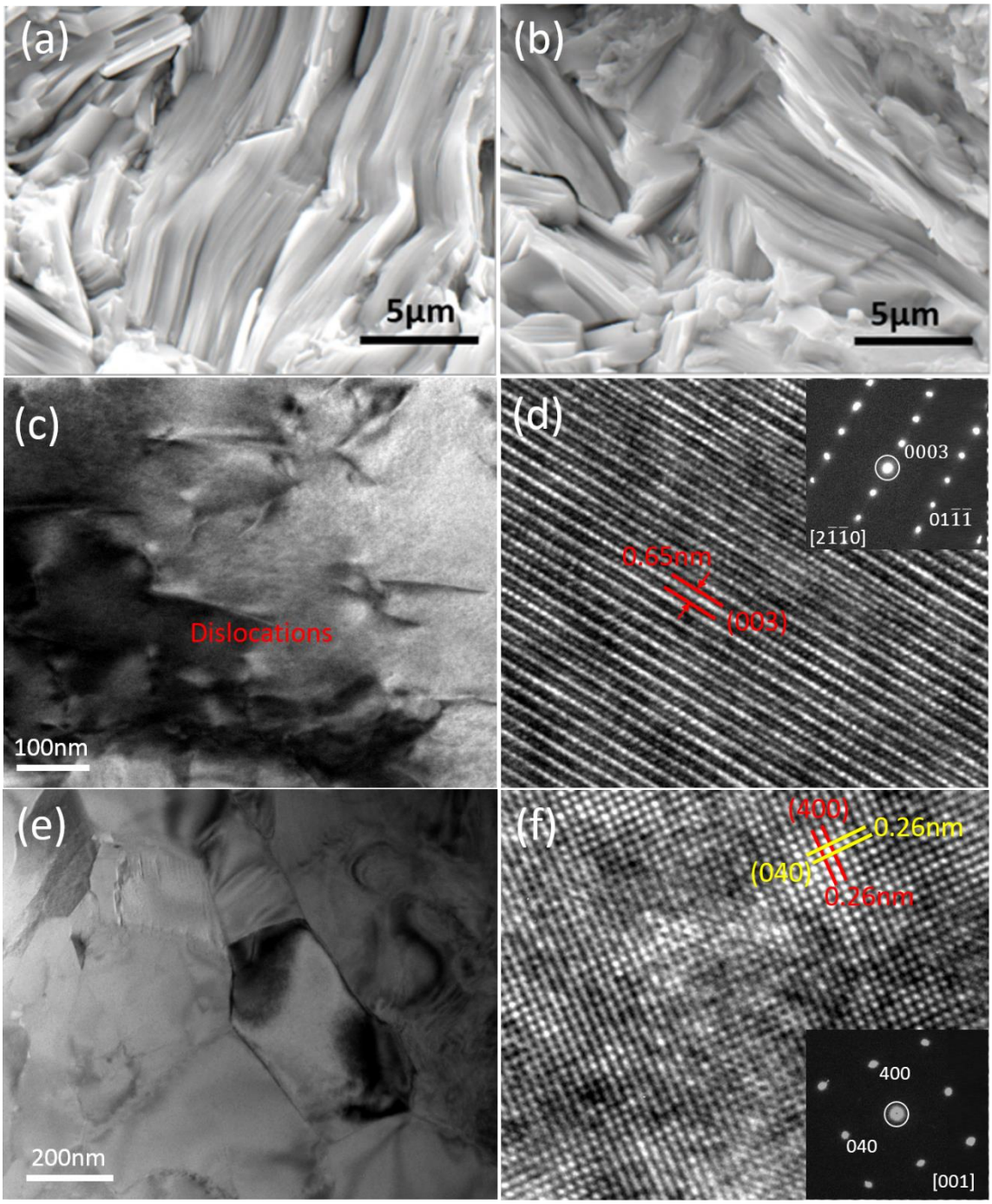

Fig. 2 SEM images of the fracture surface of samples sintered at (a) 873*K*, (b) 1023*K*. Transmission electron microscope (TEM) images of samples sintered at 873*K* and 1023*K* for bulk $CuCrSe_2$, images (c) and (d) are for sample SPS at 1023*K* showing the hexagonal phase, images (e) and (f) are for sample SPS at 873*K* showing the extra cubic phase in addition to the hexagonal phase.

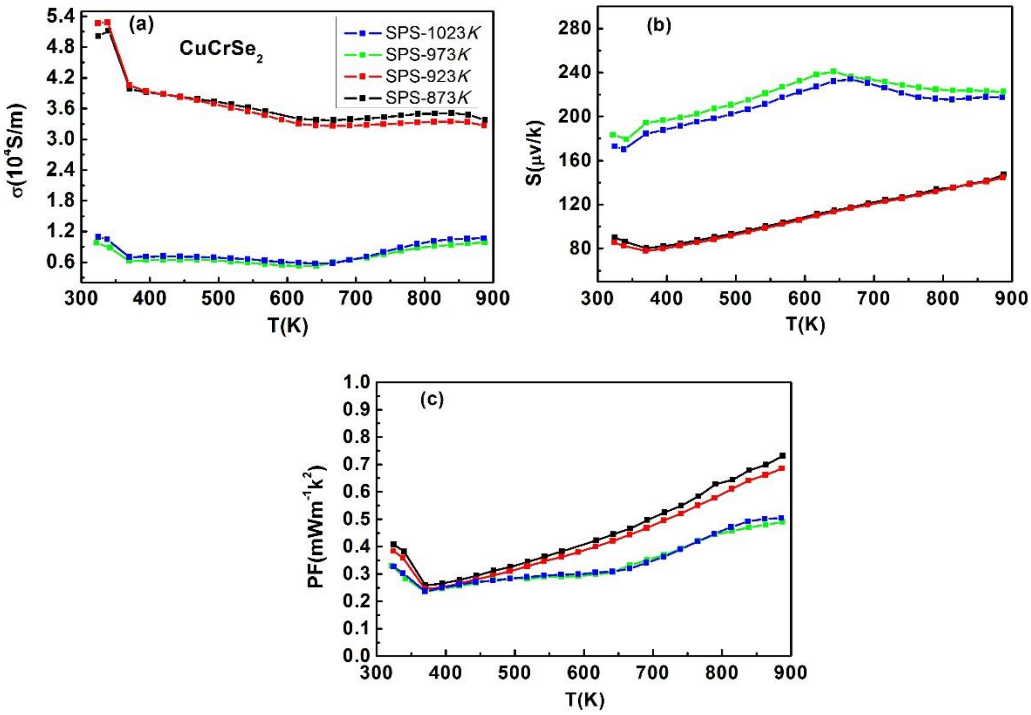

Fig 3. Temperature dependences of the electronic transport properties of all samples sintered at 873*K*, 923*K*, 973*K* and 1023*K*: (a) electrical conductivity. (b) Seebeck coefficient. (c) Power factor. The observed abnormalities at ~365 *K* indicate the onset of the disorder of Cu^{+} in $CuCrSe_2$.

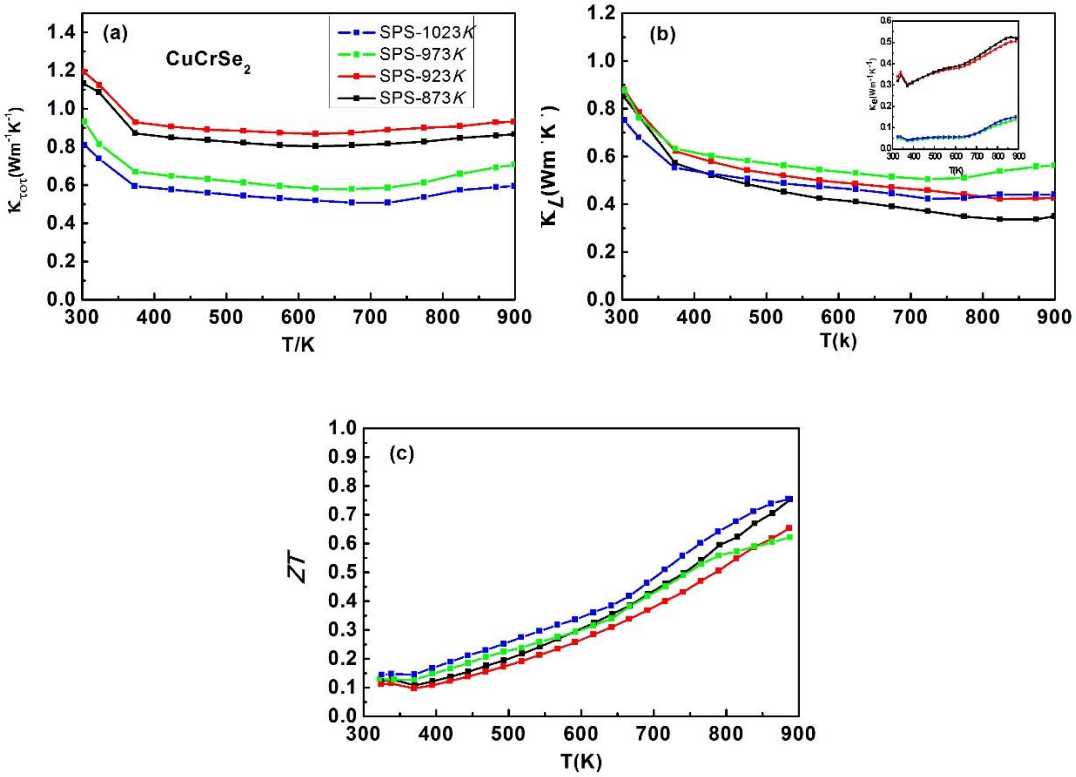

Fig. 4 Temperature dependence of all samples: (a) total thermal conductivity. (b) lattice thermal conductivity. (c) dimensionless figure of merit *ZT* for samples sintered at 873*K*, 923*K*, 973*K* and 1023*K*.

Supplementary Material

Sintering temperature dependence of thermoelectric performance in $CuCrSe_2$ prepared via mechanical alloying

Yanci Yan[a], Lijie Guo[a], Zhi Zhang[c], Xu Lu[a], Kunling Peng[a,b], Wei Yao[a], Jiyan Dai[c], Guoyu Wang[b], Xiaoyuan Zhou[a]*

[a]College of Physics, Chongqing University, Chongqing 401331, People's Republic of China.

[b]Chongqing Institute of Green and Intelligent Technology, Chinese Academy of Sciences, Chongqing 400714, People's Republic of China.

[c]Department of Applied Physics, The Hong Kong Polytechnic University, Kowloon, Hong Kong, China

*To whom correspondence should be addressed:

Author Email: xiaoyuan2013@cqu.edu.cn

1. Phase diagram of Cu-Cr-Se system

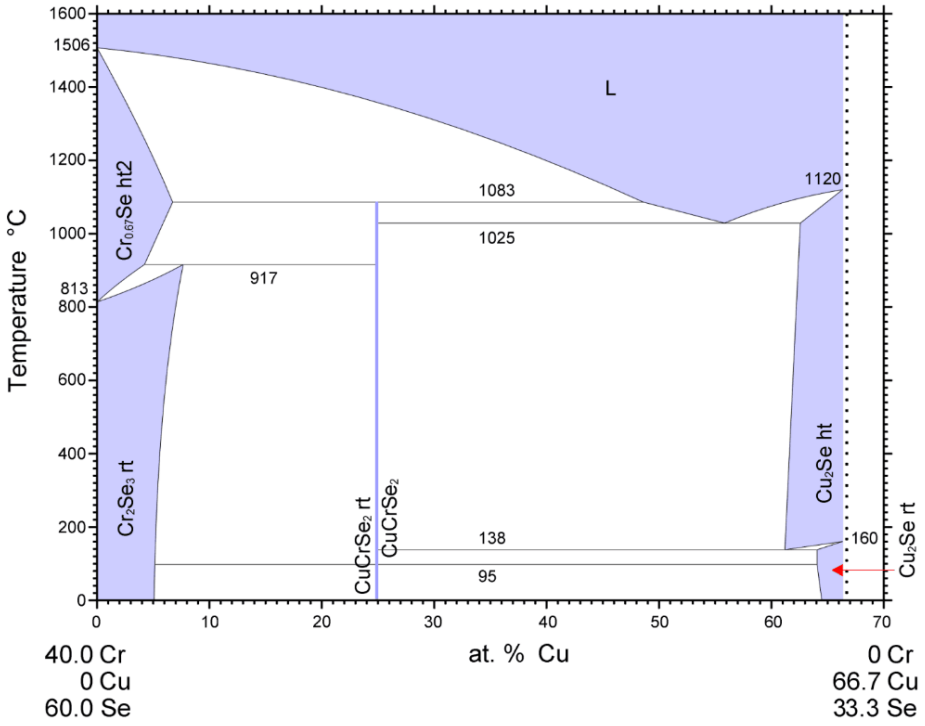

Fig. S1 Phase diagram of Cu-Cr-Se system.